

and the NTGs, in the direction of the C–C bond between the carbonyl carbon and the aromatic ring. The position of the carbonyl carbon is defined by the angle ϕ (-63°) and is consistent with α -helical structure at the NH_2 -terminus and a hydrogen bond between the probe carbonyl oxygen and the amide NH of residue 4 (1). The charge on SUC is placed 3.5 Å from the amide nitrogen atom of residue 3 in the direction of the N–H bond. The calculated backbone-charge interaction energy for a 41-residue Ala α helix is larger than for the 21-residue helix by $\sim 11\%$ for the charge position assumed for MABA and TPA and by $\sim 5\%$ for SUC.

19. C. Tanford and J. G. Kirkwood, *J. Am. Chem. Soc.* **79**, 5333 (1957); D. C. Rees, *J. Mol. Biol.* **141**, 323 (1980); J. A. Wells, D. B. Powers, R. R. Bott, T. P. Graycar, D. A. Estell, *Proc. Natl. Acad. Sci. U.S.A.* **84**, 1219 (1987).
20. M. K. Gilson, A. Rashin, R. Fine, B. Honig, *J. Mol. Biol.* **183**, 503 (1985).
21. The negative charge on the deprotonated SUC group interacts favorably with the helical backbone, and this may result in restriction of rotation about some of the succinyl C–C single bonds. Restricted motion is suggested by an increase in the intensity of NOEs between the SUC methylene protons and the β protons of residue 3 when the group is negatively charged (D. J. Lockhart and P. S. Kim, unpublished results). Because of this possible entropic contribution, the measured value of $\Delta\Delta G_p$ for SUC is a lower limit for the strength of the purely electrostatic interaction between the negative charge and the backbone, and the ϵ_{eff} value of 95 is an upper limit.
22. Neutral MABA is somewhat dipolar, and the dipole moment is approximately aligned with the electric field produced by the helix (1). Protonated MABA, however, is expected to be less dipolar because of the reduced importance of charge-separated resonance forms. Thus, there is an additional unfavorable electronic contribution to the free energy of protonation of MABA in the presence of helical structure, and the ϵ_{eff} value of 40 calculated from the MABA $\text{p}K_a$ shift data is a lower limit. Given a physically reasonable upper limit of ~ 100 , the ϵ_{eff} values obtained from the $\Delta\text{p}K_a$ data for all three titratable probe groups are qualitatively consistent.
23. F. H. Westheimer and J. G. Kirkwood, *J. Chem. Phys.* **6**, 513 (1938).
24. F. W. Baker, R. C. Parish, L. M. Stock, *J. Am. Chem. Soc.* **89**, 5677 (1967).
25. Measurements on benzyl aspartate polymers (with polar groups at the para position of the benzyl group) suggest that interactions between dipolar side chains and the helix backbone can be significant in determining the helical sense of the polymer [A. Wada, *Adv. Biophys.* **9**, 1 (1976)]. The stability of a neutral helix has been observed to increase linearly with ionic strength [J. M. Scholtz *et al.*, *J. Am. Chem. Soc.* **113**, 5102 (1991)].
26. J. G. Kirkwood, *J. Chem. Phys.* **2**, 351 (1934); T. L. Hill, *J. Phys. Chem.* **60**, 253 (1956); S. Ehrenson, *J. Am. Chem. Soc.* **98**, 7510 (1976); J. Warwicker and H. C. Watson, *J. Mol. Biol.* **157**, 671 (1982); D. Bashford and M. Karplus, *Biochemistry* **29**, 10219 (1990).
27. For a point dipole, the electric field is inversely proportional to the distance cubed and the electrostatic potential is inversely proportional to the distance squared. For a charge, the electric field is inversely proportional to distance squared and the potential is inversely proportional to distance to the first power.
28. We note that the center of the dipolar charge distribution for the neutral dipolar probe (MABA) used previously (1) is not located at exactly the same position as the center of the charges on MABA and TPA. Although it is difficult to evaluate the effect of this difference, it is not expected to be a dominant factor in determining differential screening effects because both the charged and dipolar groups used here are highly accessible to solvent.
29. T. Sakamoto, H. Nakamura, H. Uedaira, A. Wada,

J. Phys. Chem. **93**, 357 (1989).

30. Y.-H. Chen, J. T. Yang, K. H. Chau, *Biochemistry* **13**, 3350 (1974).
31. We thank R. Rutkowski, M. Milhollen, and M. Burgess for peptide synthesis, attachment of the probes, and mass spectrometry; S. Stradley for amino acid analysis; Z. Peng and L. McIntosh for help with NMR; B. Tidor for help with CHARMM; and

B. Tidor, Z. Peng, J. Weissman, and P. Petillo for helpful discussions. D.J.L. is supported by a Damon Runyon–Walter Winchell Cancer Research Fund Fellowship. P.S.K. is a Pew Scholar in the Biomedical Sciences. Supported by the Howard Hughes Medical Institute.

6 November 1992; accepted 28 January 1993

Pressure-Induced Amorphization of $R\text{-Al}_5\text{Li}_3\text{Cu}$: A Structural Relation Among Amorphous Metals, Quasi-Crystals, and Curved Space

Robert R. Winters and William S. Hammack*

A central question in the study of amorphous materials is the extent to which they are ordered. When the crystalline intermetallic $R\text{-Al}_5\text{Li}_3\text{Cu}$ is compressed to 23.2 gigapascals at ambient temperature, an amorphous phase is produced whose order can be described as defects in a curved-space crystal. This result supports a structural relation between quasi-crystals and amorphous metals based on icosahedral ordering. This result also shows that a metallic crystal can be made amorphous by compression.

A central question in the study of amorphous materials is: "How disordered are they?" (1). Formally this is known as the problem of medium-range order (MRO), that is, order on the length scale 5 to 20 Å. Experimentally MRO is difficult to measure, although recent work has shown conclusively ordering to ~ 10 Å for an alkali silicate glass (2). Also, the phenomenon of pressure-induced amorphization, a new method for preparing amorphous solids at ambient temperature by compression, has demonstrated a sense of order in amorphous solids (3–9). The difficult aspect is how to describe this "new" order in amorphous materials. The most common approach is to establish the short-range order in the amorphous material and then look for the topological rules that govern the MRO (10).

Several researchers have proposed that the order in amorphous metals can be found by examining a perfect crystal formed in a curved space (11, 12). Sadoc and Rivier showed how de-curving this perfect crystal can produce a metal alloy or an amorphous metallic structure (13). Similarly, Nelson used the perfect curved-space crystal to define defects in icosahedral bond orientational order (11). The major point of their work was to change the level at which disorder is considered. Rather than focusing on the irregular arrangement of atoms, one focuses on the structure of the defects because they are defined relative to a perfect state in curved space.

In this work we show that compression

can produce an amorphous metallic alloy whose order is described in curved space. Moreover, this result shows that we have observed the pressure-induced amorphization of a crystalline metal. The preparatory method is also unusual because the amorphous solid is produced without quenching: typically ultrahigh quench rates, on the order of 10^6 °C/s, are needed to produce amorphous metals (10).

To understand the curved-space ideas mentioned above, we must review several packing principles of metallic alloys. Metallic alloys prefer to have a coordination shell of 12 atoms in the shape of an icosahedron (14, 15). This arrangement allows the densest local packing and hence the lowest energy (16). A crystal consisting of only perfect icosahedral coordination shells is incompatible with space-filling requirements; this balance between locally low-energy noncrystallographic packings and long-range periodicity has been called "topological frustration" (8, 17). Nature adjusts this frustration by mixing different coordination shells— coordinations of 14, 15, or 16 atoms—forming what are called Frank-Kasper phases (18, 19). These alloys are composed of atoms of different sizes. Thus, purely tetrahedral packing is allowed, which results in a more efficient packing than cubic or hexagonal close packing. Because the Frank-Kasper phases have only slightly distorted tetrahedral interstices, they are often called tetrahedrally close-packed (tcp) structures (14).

A structure does exist in a curved space, however, in which every atom has perfect icosahedral coordination; it is called polytope {3,3,5}. It can be regarded as a four-dimensional analog of the regular icosahed-

Department of Chemical Engineering, Carnegie Mellon University, Pittsburgh, PA 15213.

*To whom correspondence should be addressed.

dron in Euclidean (flat) space. Sadoc and Mosseri have shown how to produce tcp structures or metallic glasses in Euclidian (flat) space by introducing defects or “disclinations” in the ideal icosahedrally ordered curved-space crystal (12). Effectively, these disclinations reduce the curvature of polytope {3,3,5}. Disclinations are defined as follows. In the higher space polytope each atom would have a coordination number of 12; this would mean that five tetrahedra are packed around each “bond.” When there are more than or fewer than five tetrahedra around a bond, then a disclination line is formed, that is, a defect in the perfect icosahedral order of curved space is created. Disclinations are formed by cutting the (higher space) structure and adding a wedge of material. This changes the number of tetrahedra around a bond to six, seven, or eight, creating a defect in the perfect icosahedral order (12). This process causes several atoms to become 14-, 15-, or 16-coordinated. By connecting these atoms one obtains the set of disclination lines necessary for flattening polytope {3,3,5}; it can then be thought of as a set of these defects. If these lines are periodic, the structure is crystalline; if they are not, it is amorphous. Frank-Kasper phases result from introducing disclinations into the higher space polytope because the phases contain atoms with only 12, 14, 15, or 16 neighbors; the latter three coordinations make up the disclination line network. As Nelson pointed out (11, p. 5516), “Upon disordering a Frank-Kasper disclination net-

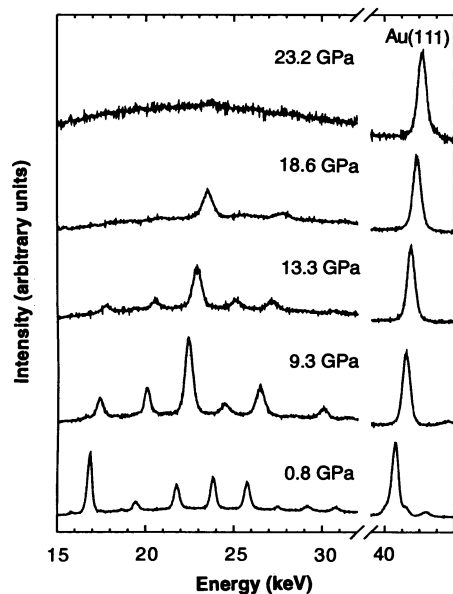


Fig. 1. Energy-dispersive x-ray diffraction patterns of crystalline $R\text{-Al}_5\text{Li}_3\text{Cu}$ at pressures of 0.8, 9.3, 13.3, 18.6, and 23.2 GPa ($E_d = 88.18 \text{ keV}\cdot\text{\AA}$). The spectra have been normalized to the intensity of the Au(111) peak, which appears at energies greater than 40 keV.

work, one obtains an attractive model for a metallic glass.” For this reason we chose to study the behavior of a Frank-Kasper phase at high pressure to see whether we could produce an amorphous metallic alloy.

Specifically we studied the intermetallic $R\text{-Al}_5\text{Li}_3\text{Cu}$ because it is closely related to the higher space polytope {3,3,5} (20). The effect of pressure on the x-ray diffraction pattern of $R\text{-Al}_5\text{Li}_3\text{Cu}$ is shown in Fig. 1 (21). The important aspects are as follows: (i) below 18 GPa the major diffraction peaks of $\text{Al}_5\text{Li}_3\text{Cu}$ can be seen; (ii) above 18 GPa the crystal structure begins to deteriorate, and only one diffraction peak is prominent; (iii) at 23.2 GPa the alloy becomes x-ray amorphous. The ambient-pressure crystal structure is recovered if the pressure is released by 18.6 GPa; upon release from 23.2 GPa the amorphous state is retained. We also measured the released amorphous sample after 4 weeks of relaxation at ambient pressure: no diffraction peaks reappeared. Compression of the crystal to a pressure of 18.6 GPa resulted in a 26% volume decrease (see Fig. 2). Because amorphization occurs at ambient temperature and shear stresses are not a significant factor in the transformation, the amorphous state has largely the topology of the original Frank-Kasper phase but with disordered disclination lines. Thus, we have created an amorphous material whose order can be described in curved space.

The amorphization occurs because there are nearly icosahedral clusters in the crystal structure of $R\text{-Al}_5\text{Li}_3\text{Cu}$ (see Fig. 3). The structure is body-centered-cubic (bcc) with a lattice constant of 13.9 \AA and 160 atoms per unit cell (22, 23). A 104-atom cluster in the shape of a truncated icosahedron (TI) is located on each bcc lattice site. This is the same shape as that of a “buckyball,” although, unlike a buckyball, these TIs are full of atoms. The interior contains 44 atoms with the same local coordination as polytope {3,3,5}, an icosahedron surrounded by a pentagonal dodecahedron. These 104-atom clusters do not have perfect icosahedral symmetry, which is incompatible with translational periodicity (23). We suggest that the nearly icosahedral 104-atom clusters become perfectly icosahedral, caus-

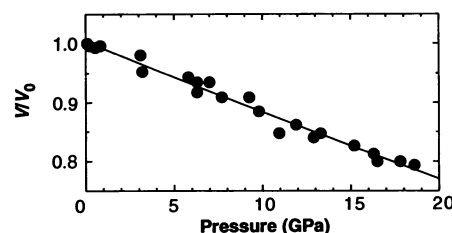


Fig. 2. The change with pressure of the volume of the unit cell of $R\text{-Al}_5\text{Li}_3\text{Cu}$. The initial volume, V_0 , is 2686 \AA^3 .

ing the amorphization; paradoxically as the structure becomes more locally ordered, the global ordering is lost. As the crystalline solid is compressed, the interatomic distances within the TI cluster decrease until a point is reached at which the interatomic repulsion is very great. At this point the atoms in the TI cluster can be repacked more efficiently into a TI with perfect icosahedral symmetry. This packing is $\sim 3\%$ more dense than the crystalline packing, but with roughly the same interatomic distances (23). A perfect TI can form only upon the loss and therefore at the expense of crystallinity. This suggests that compression can provide the energy necessary for the sample to rearrange into an amorphous state. Note from Fig. 2 that $\sim 230 \text{ kJ/mol}$ of energy is transmitted to the sample through

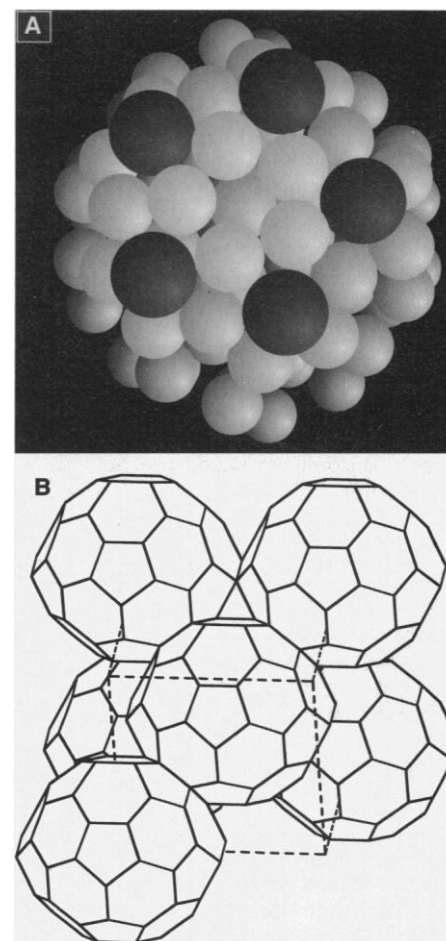


Fig. 3. (A) The truncated icosahedron (TI) characteristic of the crystal structure of $R\text{-Al}_5\text{Li}_3\text{Cu}$. The light-colored atoms are aluminum or copper and the larger dark atoms are lithium. The five light atoms in the center of the cluster form a nearly regular pentagonal ring. (B) The TIs are centered on the sites of a bcc lattice. The unit cell is shown with dotted lines. The vertices of the truncated icosahedra shown here correspond to the light-colored atoms in (A); the lithium atoms between the TI units are not shown.

pressure-volume (pV) work.

The pressure-induced amorphization of $R\text{-Al}_5\text{Li}_3\text{Cu}$ supports a suggestion of a structural relation between quasi-crystals and amorphous metals. Nelson and Spaepen have suggested that the ordering in quasi-crystals and metallic glasses is based on polytetrahedral packings like the icosahedron (17). This relation can be shown by examining the close structural relation among crystalline $R\text{-Al}_5\text{Li}_3\text{Cu}$, quasi-crystalline $i\text{-Al}_6\text{Li}_3\text{Cu}$, and the pressure-induced amorphous phase of $R\text{-Al}_5\text{Li}_3\text{Cu}$ (24). Extended x-ray absorption fine structure (EXAFS) measurements show that the icosahedral clusters in the quasi-crystal $i\text{-Al}_6\text{Li}_3\text{Cu}$ are similar to those in its crystalline counterpart $R\text{-Al}_5\text{Li}_3\text{Cu}$ except that they are more locally ordered (25). Single-crystal structural refinements of $i\text{-Al}_6\text{Li}_3\text{Cu}$ show the same atomic shells as in the R -phase (26). The measurements reported here suggest that the amorphous metallic phase $R\text{-Al}_5\text{Li}_3\text{Cu}$ created by compression has the topology of the crystalline R -phase, with more nearly perfect local icosahedral order. In addition, $i\text{-Al}_6\text{Li}_3\text{Cu}$ shows behavior similar to that of the crystalline R -phase when compressed; it undergoes a phase transition by way of a disordered state (27). These observations provide support for a close structural relation between the quasi-crystalline i -phase and the pressure-amorphized R -phase.

Our results show that we can produce an amorphous metal, at ambient temperature, by compression. Because the change is largely isoconfigurational, the amorphous state arises from the disordering of the disclination lines of a Frank-Kasper phase. Thus, the order present in the amorphous state can be described in a curved or higher dimensional space. The pressure-amorphized material is not necessarily a glass in the traditional sense: A glass is formed by the continuous solidification from the melt and exhibits a glass transition (10, 28). How is this pressure-amorphized material related to an amorphous metal produced by quenching from the melt? We speculate that it is an "ideal" glassy state and that melt-quenched metals are, owing to kinetic constraints, defective forms of amorphous materials formed by projections from curved space (29).

REFERENCES AND NOTES

1. S. R. Elliott, *Nature* **354**, 445 (1991).
2. P. H. Gaskell, M. C. Eckersley, A. C. Barnes, P. Chieux, *ibid.* **350**, 675 (1991).
3. I. Amato, *Science* **252**, 1377 (1991).
4. Y. Fujii, M. Kowaka, A. Onodera, *J. Phys. C* **18**, 789 (1985).
5. R. J. Hemley, A. P. Jephcoat, H. K. Mao, L. C. Ming, M. H. Manghnani, *Nature* **334**, 52 (1988).
6. M. B. Kruger, Q. Williams, R. Jeanloz, *J. Chem. Phys.* **91**, 5910 (1989).
7. G. C. Serghiou, R. R. Winters, W. S. Hammack,

- Phys. Rev. Lett.* **68**, 3311 (1992).
8. We have suggested elsewhere [R. R. Winters, G. C. Serghiou, W. S. Hammack, *Phys. Rev. B* **46**, 2792 (1992)] that topological frustration based on polytetrahedral packings is crucial in understanding the pressure-induced amorphization of nondirectionally bonded solids. The results presented here are an implementation of this idea.
9. R. R. Winters, A. Garg, W. S. Hammack, *Phys. Rev. Lett.* **69**, 3751 (1992).
10. P. Chaudhari and D. Turnbull, *Science* **199**, 11 (1978).
11. D. R. Nelson, *Phys. Rev. B* **28**, 5515 (1983).
12. J. F. Sadoc and R. Mosseri, *Philos. Mag. B* **45**, 467 (1982).
13. J. F. Sadoc and N. Rivier, *ibid.* **55**, 537 (1987).
14. D. P. Shoemaker and C. B. Shoemaker, in *Aperiodicity and Order: Introduction to Quasicrystals*, M. V. Jaric, Ed. (Academic Press, New York, 1988), p. 1.
15. S. Samson, in *Structural Chemistry and Molecular Biology*, A. Rich and N. Davidson, Eds. (Freeman, San Francisco, 1968), p. 687.
16. M. R. Hoare and P. Pal, *Adv. Phys.* **20**, 161 (1971).
17. D. R. Nelson and F. Spaepen, *Solid State Phys.* **42**, 1 (1989).
18. F. C. Frank and J. C. Kasper, *Acta Crystallogr.* **11**, 184 (1958).
19. ———, *ibid.* **12**, 483 (1959).
20. M. Widom, in *Aperiodicity and Order: Introduction to Quasicrystals*, M. V. Jaric, Ed. (Academic Press, New York, 1988), p. 59.
21. The sample of $R\text{-Al}_5\text{Li}_3\text{Cu}$ was obtained from F. Gayle of the National Institute of Standards and Technology. A modified Merrill-Bassett style diamond anvil cell (DAC) was used to generate high pressures [L. Merrill and W. A. Bassett, *Rev. Sci. Instrum.* **45**, 290 (1974)]; both a 4:1 methanol-ethanol mixture and argon were used as pressure-transmitting media. The same result was obtained in both media. Observing the same effect for both media implies that the amorphization is not principally due to shear [H. K. Mao, J. Xu, P. M. Bell, *J. Geophys. Res.* **91**, 4673 (1986)]. The x-ray diffraction patterns were measured by energy-dispersive x-ray diffraction (EDXD) at the Cornell High Energy Synchrotron Source (CHESS) with a germanium solid-state detector [M. A.

Baublitz, V. Arnold, A. L. Ruoff, *Rev. Sci. Instrum.* **52**, 1616 (1981); K. Brister, Y. K. Vohra, A. L. Ruoff, *ibid.* **57**, 2560 (1986)]. For all measurements Ed was 88.18 keV-Å. ($Ed = 6.1993 \text{ keV-Å} / \sin \theta$, where θ is the acute angle between the incoming x-ray radiation and the detector). We monitored the pressure by mixing gold powder (Alpha, 99.95% pure; grain size, 1 to 3 μm) with the sample. The change in the (111) diffraction line of gold was monitored, and the pressure was then calculated with an equation of state [D. L. Heinz and R. Jeanloz, *J. Appl. Phys.* **55**, 885 (1984)]. The gold also served to indicate that we had truly lost the diffraction patterns of the samples and had not erred in aligning the DAC with the synchrotron beam.

22. M. Audier *et al.*, *Physica B* **153**, 136 (1988).
23. C. A. Guryan, P. W. Stephens, A. I. Goldman, F. W. Gayle, *Phys. Rev. B* **37**, 8495 (1988).
24. B. Dubost, J.-M. Lang, M. Tanaka, P. Sainfort, M. Audier, *Nature* **324**, 48 (1986).
25. Y. Ma, E. A. Stern, F. W. Gayle, *Phys. Rev. Lett.* **58**, 1956 (1987).
26. M. de Boissieu, C. Janot, J. M. Dubios, M. Audier, B. Dubost, *J. Phys. Condensed Matter* **3**, 1 (1991).
27. Y. Akahama, *et al.*, *J. Phys. Soc. Jpn.* **58**, 2231 (1989).
28. J. Zarzycki, *Glasses and the Vitreous State* (Cambridge Univ. Press, Cambridge, 1991).
29. For example, J. C. Phillips has pointed out that the icosahedral ordering models ignore the influence of quenching kinetics and mechanical stability that are seminal in the formation of a rapidly quenched metal [*J. Mater. Res.* **1**, 1 (1986)]. The preparatory methods used here bypass these considerations.
30. This work was supported by the Division of Materials Sciences, Office of Basic Energy Sciences, Department of Energy, under contract DE-FG02-92ER45474. We thank K. Brister and the staff at CHESS for their assistance with the high-pressure EDXD experiments, M. Widom and J. Robeson for critical comments, and F. Gayle for providing the sample of $R\text{-Al}_5\text{Li}_3\text{Cu}$.

3 November 1992; accepted 21 January 1993

Velocity Structure of a Gas Hydrate Reflector

Satish C. Singh, Timothy A. Minshull, George D. Spence

Seismic reflection profiles across many continental margins have imaged bottom-simulating reflectors (BSRs) parallel to the seabed; these are often interpreted as the base of a zone in which methane hydrate "ice" is stable. Waveform inversion of seismic reflection data can be used to estimate from seismic data worldwide the velocity structure of a BSR and its thickness. A test of this method at a drill site of the Ocean Drilling Program predicts that sediment pores beneath the BSR contain free methane for approximately 30 meters. The hydrate and underlying gas represent a large global reservoir of methane, which may have economic importance and may influence global climate.

Bottom-simulating reflectors (BSRs) are found in the upper few hundred meters of ocean bottom sediments on and adjacent to

many continental margins. They are most often found in accretionary sediment prisms at convergent continental margins. BSRs have been widely interpreted as marking the base of the zone in which methane hydrate is stable (1); methane hydrate stability is primarily temperature-controlled under these conditions and therefore the base of this zone follows local isotherms. As such, BSRs have been used to estimate thermal gradient and hence heat flow (2, 3). However, BSRs have wider significance

S. C. Singh, British Institutions Reflection Profiling Syndicate, Bullard Laboratories, University of Cambridge, Madingley Road, Cambridge CB3 0EZ, United Kingdom.
T. A. Minshull, Bullard Laboratories, University of Cambridge, Madingley Road, Cambridge CB3 0EZ, United Kingdom.
G. D. Spence, School of Ocean and Earth Sciences, University of Victoria, Victoria, British Columbia V8W 2Y2, Canada.